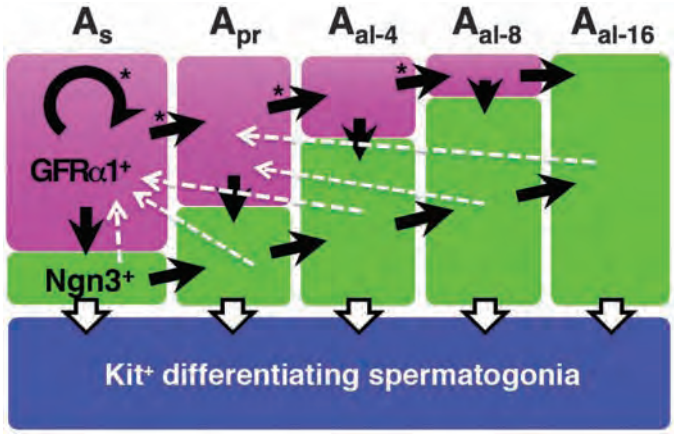

Fig. 6. Proposed spermatogonial subpopulations and their behavior with respect to their morphology (cyst length) and gene expression (GFRα1$^+$ and NGN3$^+$). Black arrows indicate the proposed flow of the majority of cells in each morphological group. Dashed lines show the observed modes of "reversion." Arrows without asterisks were actually observed; those with asterisks were not observed but are proposed to occur with high probability.

gonia proliferate actively, the cell cycle status of GFRα1$^+$ population is yet to be elucidated. It is an intriguing question whether there exists a reserve population of GFRα1$^+$ cells in mice, equivalent to the A_{dark} cells in primates, or whether a reserve population of stem cells is unique to primates.

The biological importance of the syncytial nature of spermatogonial proliferation across animal species remains a mystery. Nonetheless, it provides a powerful tool to monitor gene expression in the context of cell lineage. In other stem cell systems, especially in mammals, stem and progenitor cell compartments are often classified on the basis of gene expression and location; correlation of lineage and gene expression has generally not been feasible. Our study demonstrates that lineage is not strictly and linearly correlated with gene expression and that there may be multiple and reversible paths from stem cells to differentiation in other systems.

References and Notes

1. S. J. Morrison, A. C. Spradling, *Cell* **132**, 598 (2008).
2. G. Seydoux, R. E. Braun, *Cell* **127**, 891 (2006).
3. M. T. Fuller, A. C. Spradling, *Science* **316**, 402 (2007).
4. C. Brawley, E. Matunis, *Science* **304**, 1331 (2004).
5. T. Kai, A. Spradling, *Nature* **428**, 564 (2004).
6. T. Nakagawa, Y. Nabeshima, S. Yoshida, *Dev. Cell* **12**, 195 (2007).
7. J. Cheng *et al.*, *Nature* **456**, 599 (2008).
8. V. Barroca *et al.*, *Nat. Cell Biol.* **11**, 190 (2008).
9. D. G. de Rooij, L. D. Russell, *J. Androl.* **21**, 776 (2000).
10. L. Russell, R. Ettlin, A. Sinha Hikim, E. Clegg, *Histological and Histopathological Evaluation of the Testis* (Cache River Press, Clearwater, FL, 1990).
11. M. L. Meistrich, M. E. van Beek, in *Cell and Molecular Biology of the Testis*, C. Desjardins, L. L. Ewing, Eds. (Oxford Univ. Press, New York, 1993), pp. 266–295.
12. S. Yoshida, *Cold Spring Harb. Symp. Quant. Biol.* **73**, 25 (2008).
13. D. G. de Rooij, *Reproduction* **121**, 347 (2001).
14. C. Huckins, *Anat. Rec.* **169**, 533 (1971).
15. E. F. Oakberg, *Anat. Rec.* **169**, 515 (1971).
16. S. Yoshida *et al.*, *Dev. Biol.* **269**, 447 (2004).
17. F. W. Buaas *et al.*, *Nat. Genet.* **36**, 647 (2004).
18. J. A. Costoya *et al.*, *Nat. Genet.* **36**, 653 (2004).
19. X. Meng *et al.*, *Science* **287**, 1489 (2000).
20. M. C. Hofmann, L. Braydich-Stolle, M. Dym, *Dev. Biol.* **279**, 114 (2005).
21. M. Tokuda, Y. Kadokawa, H. Kurahashi, T. Marunouchi, *Biol. Reprod.* **76**, 130 (2007).
22. H. Suzuki, A. Sada, S. Yoshida, Y. Saga, *Dev. Biol.* **336**, 222 (2009).
23. K. Zheng, X. Wu, K. H. Kaestner, P. J. Wang, *BMC Dev. Biol.* **9**, 38 (2009).
24. S. Yoshida, M. Sukeno, Y. Nabeshima, *Science* **317**, 1722 (2007).
25. B. H. Schrans-Stassen, H. J. van de Kant, D. G. de Rooij, A. M. van Pelt, *Endocrinology* **140**, 5894 (1999).
26. B. H. Erickson, *Radiat. Res.* **86**, 34 (1981).
27. J. Ehmcke, C. M. Luetjens, S. Schlatt, *Biol. Reprod.* **72**, 293 (2005).
28. J. Ehmcke, S. Schlatt, *Reproduction* **132**, 673 (2006).
29. D. G. de Rooij, *Int. J. Exp. Pathol.* **79**, 67 (1998).
30. R. L. Brinster, *Science* **296**, 2174 (2002).
31. C. S. Potten, M. Loeffler, *Development* **110**, 1001 (1990).
32. J. M. Oatley, M. R. Avarbock, A. I. Telaranta, D. T. Fearon, R. L. Brinster, *Proc. Natl. Acad. Sci. U.S.A.* **103**, 9524 (2006).
33. M. Kanatsu-Shinohara *et al.*, *Biol. Reprod.* **69**, 612 (2003).
34. H. Kubota, M. R. Avarbock, R. L. Brinster, *Proc. Natl. Acad. Sci. U.S.A.* **101**, 16489 (2004).

35. We thank J. Miyazaki, T. Noce, and A. Imura for materials; T. Ogawa, R. Sugimoto, Y. Kitadate, K. Hara, and H. Mizuguchi-Takase for comments; T. Fujimori for discussion and technical advice; and M. Sukeno for technical assistance. Supported by a Grant-in-Aid for Scientific Research (KAKENHI) on Innovative Areas, "Regulatory Mechanism of Gamete Stem Cells" (S.Y.), NICHD/NIH Contraceptive Development Research Centers Program grant U54 HD4254 (R.E.B.), the Uehara Memorial Foundation, and the Naito Foundation.

Supporting Online Material

www.sciencemag.org/cgi/content/full/science.1182868/DC1
Materials and Methods
SOM Text
Figs. S1 to S7
Movies S1 to S4
References

5 October 2009; accepted 1 March 2010
Published online 18 March 2010;
10.1126/science.1182868
Include this information when citing this paper.

A Gating Charge Transfer Center in Voltage Sensors

Xiao Tao,[1] Alice Lee,[1] Walrati Limapichat,[2] Dennis A. Dougherty,[2] Roderick MacKinnon[1]*

Voltage sensors regulate the conformations of voltage-dependent ion channels and enzymes. Their nearly switchlike response as a function of membrane voltage comes from the movement of positively charged amino acids, arginine or lysine, across the membrane field. We used mutations with natural and unnatural amino acids, electrophysiological recordings, and x-ray crystallography to identify a charge transfer center in voltage sensors that facilitates this movement. This center consists of a rigid cyclic "cap" and two negatively charged amino acids to interact with a positive charge. Specific mutations induce a preference for lysine relative to arginine. By placing lysine at specific locations, the voltage sensor can be stabilized in different conformations, which enables a dissection of voltage sensor movements and their relation to ion channel opening.

Voltage sensors are membrane proteins that change their conformation in response to voltage differences across the cell membrane. They are best known as components of voltage-dependent ion channels, in which voltage sensor conformational changes regulate channel opening. Voltage-dependent K^+ (Kv) and Na^+ (Nav) channels produce nerve impulses, and voltage-dependent Ca^{2+} (Cav) channels initiate muscle contraction and many other cellular processes (*1*). Certain enzymes also have voltage sensors, which allow the membrane voltage to regulate catalytic activity (*2*, *3*).

Voltage sensors can exhibit a nearly switch-like dependence on membrane voltage, changing from "off" to "on" over a few hundredths of a volt. Such a steep dependence on voltage exists because a large quantity of electric charge (known as gating charge) is transferred across the membrane voltage difference when a sensor switches off to on (*4*). In the Shaker Kv channel, the total gating charge is 12 to 14 elementary charges per channel, or 3.0 to 3.5 elementary charges from each of four voltage sensors (*5*–*7*). The charges originate from amino acids carrying a positive charge—mostly arginine but occasionally lysine—located on the fourth membrane-spanning helix (S4) of the voltage sensor (*5*, *6*).

[1]Laboratory of Molecular Neurobiology and Biophysics, Rockefeller University, Howard Hughes Medical Institute, 1230 York Avenue, New York, NY 10065, USA. [2]Division of Chemistry and Chemical Engineering, California Institute of Technology, 1200 East California Boulevard, Pasadena, CA 91125, USA.

*To whom correspondence should be addressed. E-mail: mackinn@rockefeller.edu

Crystal structures of voltage sensors from Kv channels show that they consist of only four transmembrane helices surrounded by the lipid membrane (*8*–*11*). The seemingly simple structure of the voltage sensor presents an apparent paradox: How does the voltage sensor transfer a large quantity of charge across the low-dielectric and charge-destabilizing interior of the membrane when there are only four helices to "shield" the charges? Some explanations have posited that the sensor does not physically move its charges very far across the membrane, but rather that it somehow restructures the electric field relative to the charges (*12*–*17*). However, other studies suggest that charged amino acids on S4 move 15 to 20 Å across the membrane (*18*–*20*). Such large movements would seem to require a specific mechanism to stabilize the charges as they cross the membrane center.

Voltage sensors of Kv channels. Kv channels consist of a central ion conduction pore surrounded by four voltage sensors (Fig. 1A) (*8*–*11*). Each voltage sensor contacts the pore through two functionally important interfaces: one located near the extracellular (top) surface of helix S1 and another near the intracellular surface at the S4-S5 linker (*21*). The segments of the voltage sensor colored red in Fig. 1A (S3b, S4, and the S4-S5 linker) are proposed to move relative to the more static segments colored gray (S1, S2, and S3a) (*18*, *22*). The crystal structure of the closed conformation has not been determined, but in a proposed mechanism, a hinge between S3a and S3b would allow the voltage sensor paddle (S3b and S4) to undergo movement, which would exert force on the S4-S5 linker to close or open the pore as modeled in Fig. 1B (*10*, *11*, *21*). The voltage difference across the membrane drives the conformational change by acting on positively charged residues on S4 (Fig. 1, C and D).

In the crystal structure of the Kv1.2-Kv2.1 chimera (paddle chimera), the pore is open, and the voltage sensors adopt a membrane depolarized (positive inside relative to outside) conformation (Fig. 1, A to C) (*11*). We refer to this depolarized voltage sensor conformation as the open voltage sensor and the hyperpolarized conformation as the closed voltage sensor. In the open crystal structure, positively charged amino acids are labeled according to their position on S4 from outside to inside, 0 to 5 (Fig. 1, C and D). Position 1 is Gln in paddle chimera but Arg in Kv1 channels such as the Shaker channel. The outermost charged amino acids, labeled R0 to R4 (*23*), are located either near the phospholipid head group layer (R0 and R1) or in an aqueous cleft created because the paddle is tilted away from S1 and S2 (R2 to R4) (Fig. 1C). R0 to R4 are, therefore, in or near an extracellular surface–exposed environment. The next positively charged amino acid, K5, is different, because it is isolated from the external aqueous surface by a phenylalanine side chain, Phe^{233} (Fig. 1C, green side chain). The Phe is highly conserved among voltage sensors from many different proteins, including Kv, Nav, Cav, voltage-dependent H^+ (Hv) channels, and voltage-dependent phosphatase (VSP) enzymes (Fig. 1E) (*24*, *25*). What role does this Phe play?

Effects of mutating Phe^{233}. To address this question, we introduced mutations in this Phe by substituting 19 other amino acids (*23*, *26*) (Fig. 2, A and B). These experiments were carried out with the Shaker K^+ channel instead of the paddle chimera channel because the Shaker channel is highly expressed in *Xenopus* oocytes, and it is the most extensively studied Kv channel with respect to gating function (*27*–*31*). Even though the crystal structure of the Shaker K^+ channel has not been determined, the paddle

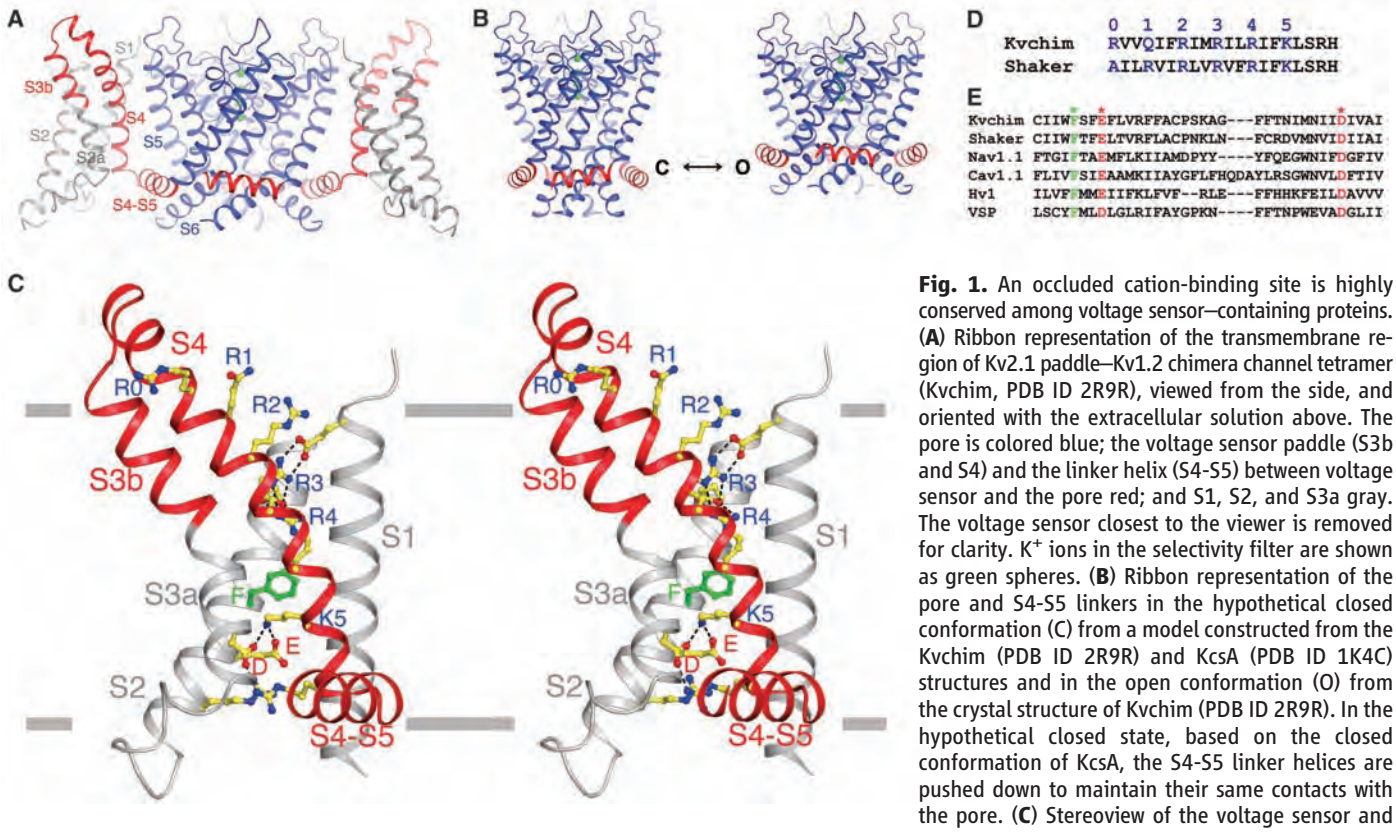

Fig. 1. An occluded cation-binding site is highly conserved among voltage sensor–containing proteins. (**A**) Ribbon representation of the transmembrane region of Kv2.1 paddle–Kv1.2 chimera channel tetramer (Kvchim, PDB ID 2R9R), viewed from the side, and oriented with the extracellular solution above. The pore is colored blue; the voltage sensor paddle (S3b and S4) and the linker helix (S4-S5) between voltage sensor and the pore red; and S1, S2, and S3a gray. The voltage sensor closest to the viewer is removed for clarity. K^+ ions in the selectivity filter are shown as green spheres. (**B**) Ribbon representation of the pore and S4-S5 linkers in the hypothetical closed conformation (C) from a model constructed from the Kvchim (PDB ID 2R9R) and KcsA (PDB ID 1K4C) structures and in the open conformation (O) from the crystal structure of Kvchim (PDB ID 2R9R). In the hypothetical closed state, based on the closed conformation of KcsA, the S4-S5 linker helices are pushed down to maintain their same contacts with the pore. (**C**) Stereoview of the voltage sensor and S4-S5 linker helix of the open conformation from Kvchim. Side chains of the positively charged residues on S4 (labeled as R0, R1, R2, R3, R4, and K5) and the negatively charged residues forming ionizing hydrogen bonds (dashed black lines) with the positive charges, as well as those of the three residues (labeled F, E, and D) forming an occluded binding site in the voltage sensor, are shown as sticks and colored according to atom types (yellow, carbon; blue, nitrogen; red, oxygen; and green, phenylalanine). (**D**) Sequence alignment of the S4 segment of Kvchim (GI: 160877792) and Shaker Kv (GI: 13432103). The positively charged residues are colored blue. Numbers [0 to 5, equivalent to those in (C)] above the sequences are used to indicate the positive charges on S4 throughout the text. (**E**) Sequence alignment of Kvchim (GI: 160877792), Shaker Kv (GI: 13432103), human Nav1.1 (GI: 115583677), human Cav1.1 (GI: 110349767), human Hv1 (GI: 91992155), and ciona VSP (GI: 76253898). Only the segment of S2 and S3a forming the occluded binding site is included. The three highly conserved residues forming the site are highlighted: F, green, and E and D, red. F corresponds to Phe^{233} in Kvchim.

chimera channel shares high sequence identity and, therefore, should serve as an accurate model for designing and analyzing experiments on the Shaker channel. The mutants fall into four groups, according to the level of expressed current and the midpoint voltage (V_m) of the activation curve (Fig. 2, A and B). Only two substitutions, Tyr and Trp, produced currents near wild-type levels with negative V_m (Fig. 2B).

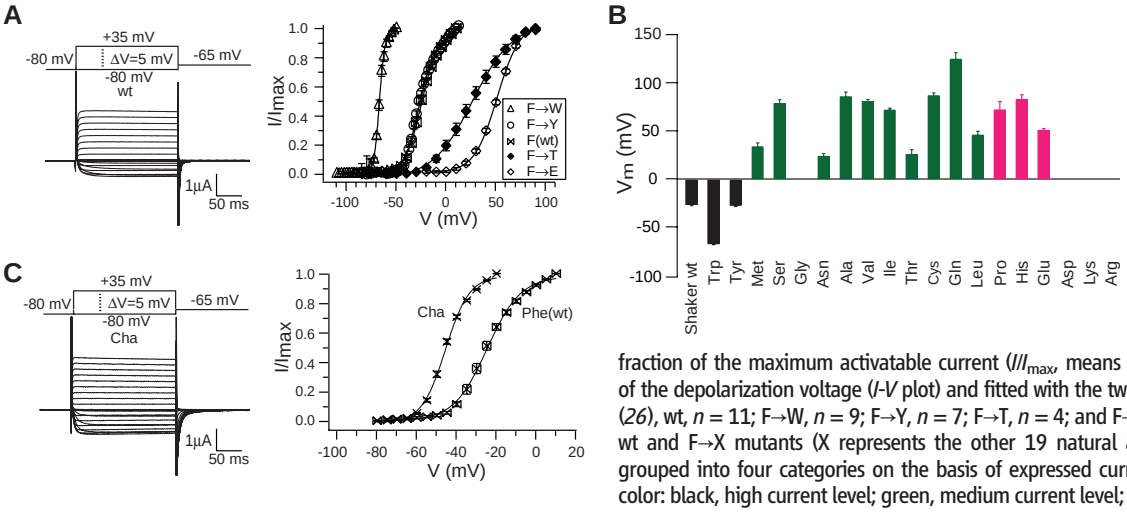

Fig. 2. A rigid cyclic side chain is important at the position of Phe^{233}. (**A**) Voltage-dependent channel activation of the Phe^{233} mutants. On the left is a representative current trace of Shaker recorded with a voltage-pulse protocol shown above. On the right, voltage activation curves of Shaker wt and F→W/Y/T/E mutants are shown, in which the fraction of the maximum activatable current (I/I_{max}, means ± SEM) is plotted as a function of the depolarization voltage (*I-V* plot) and fitted with the two-state Boltzmann function [see (*26*), wt, $n = 11$; F→W, $n = 9$; F→Y, $n = 7$; F→T, $n = 4$; and F→E, $n = 9$]. (**B**) The V_m of Shaker wt and F→X mutants (X represents the other 19 natural amino acids). The mutants are grouped into four categories on the basis of expressed current level (indicated by the bar color: black, high current level; green, medium current level; magenta, low current level) and the value of V_m (indicated by the bar height). Oocytes expressing the Lys or Arg mutants did not produce any Agitoxin2-sensitive current. The expressed current level of the Asp mutant was too low to generate a usable *I-V* plot. V_m of the Gly mutant was not determined, as its *I-V* plot cannot be fitted with the two-state Boltzmann function. (**C**) Voltage-dependent channel activation of the Phe to cyclohexylalanine (Cha) mutant. (Left) A representative current trace of the Cha mutant recorded with a voltage-pulse protocol shown above. (Right) The voltage activation curves of Shaker wt and the Cha mutant. The curves are fitted with the two-state Boltzmann function [see (*26*), wt, $n = 11$; Cha, $n = 15$].

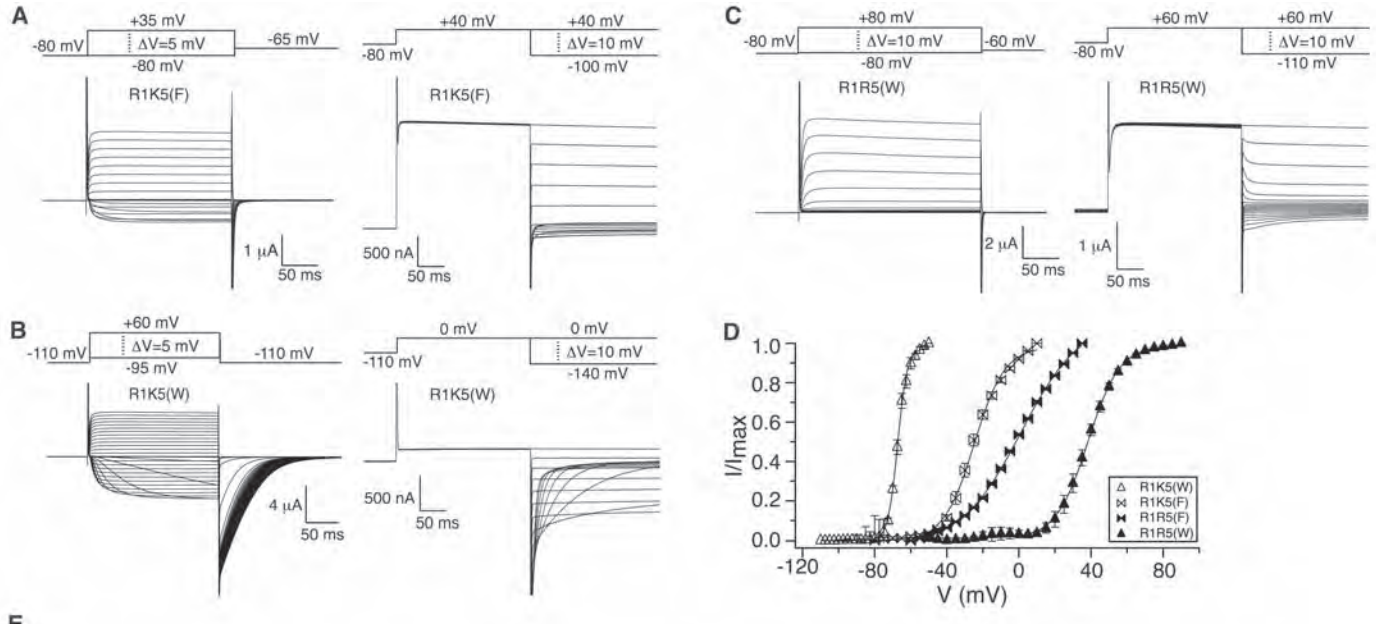

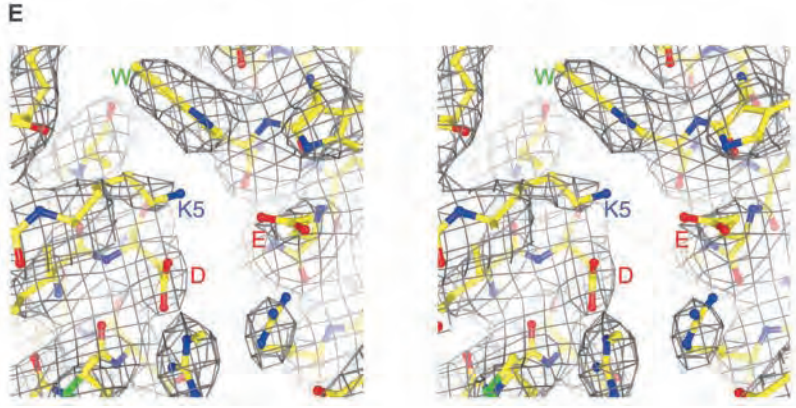

Fig. 3. Effects of the Phe to Trp mutation depend on the amino acid at position 5. (**A** to **C**) Representative current traces of voltage-dependent channel opening (left) and closing (right) of R1K5(F) (i.e., Shaker wt), R1K5(W), and R1R5(W). The corresponding pulse protocols are shown above the traces. (**D**) The voltage-activation curves of R1K5(F) (i.e., Shaker wt), R1K5(W), R1R5(F), and R1R5(W). Fraction of the maximal current (I/I_{max}, means ± SEM) is plotted as a function of the depolarization voltage and fitted with the two-state Boltzmann function [see (*26*), R1K5(F), $n = 11$; R1K5(W), $n = 9$; R1R5(F), $n = 12$; and R1R5(W), $n = 5$]. (**E**) Stereo representation of electron density (gray wire mesh, $2F_{obs} - F_{calc}$, calculated from 50 to 2.9 Å by using phases from the final model and contoured at 0.8 σ) for the occluded binding site in the crystal structure of the Kvchim F233W mutant [equivalent to R1K5(W)]. The protein is shown as sticks and colored according to atom types (yellow, carbon; blue, nitrogen; and red, oxygen).

The three amino acids with a permanent aromatic side chain (Phe, Tyr, and Trp) support the highest current levels and negative V_m. To test the importance of aromaticity and the possible existence of a cation-π interaction, we substituted Phe with cyclohexylalanine (Cha), which has a rigid cyclic side chain but is not aromatic. This mutant yielded functional channels with a negative V_m, much like channels with Phe, Tyr, and Trp (Fig. 2C). In addition, a variety of unnatural amino acid analogs of Phe, including 3,5-difluoro-Phe (F_2Phe), 4-methyl-Phe (MePhe), 4-cyano-Phe (CNPhe), and 4-bromo-Phe (BrPhe), consistently produced negative V_m values but did not show a systematic correlation with the negative electrostatic potential on the surface of the aromatic ring (fig. S1). These results suggest that a rigid cyclic side chain is important at this position, but aromaticity is not.

The channel containing Trp activates with the most negative V_m (Fig. 2, A and B). The channel kinetics underlying the more negative V_m in the Trp mutant can be seen with a voltage protocol in which the membrane is depolarized to open the channels and then hyperpolarized to close them; the rate of closure is extremely slow (Fig. 3, A and B). In general, the rate of closure is voltage dependent; it becomes faster as the membrane voltage is made more negative (right side of Fig. 3, A and B). In the wild-type channel [R1K5(F), corresponding to Arg at position 1 and Lys at position 5 on S4 (Fig. 1D), and Phe at the equivalent position of Phe^{233} on S2 (Fig. 1E)], closure is so rapid that a voltage of –65 mV is sufficient to close channels in a brief period of time (Fig. 3A). But when Phe^{233} is replaced by Trp [R1K5(W)] even at –110 mV (a voltage at which closure is expected to be much faster than at –65 mV), the channels take much longer to close (Fig. 3B). The negative V_m and slow closure suggest that the Phe to Trp mutation energetically favors the open channel relative to the closed channel.

Effects of the Phe to Trp mutation depend on the K5 amino acid. The effects of mutating Phe to Trp depend on the nature of the amino acid at position 5 (Fig. 3, A to C). This dependence can be seen through a comparison of double mutants: The R1K5(W) channel has a more negative V_m and a slower rate of closure compared with the R1K5(F) channel (Fig. 3, A, B, and D), but the R1R5(W) channel has a more positive V_m and a faster rate of closure than the R1R5(F) channel (Fig. 3, C and D, and fig. S2A). Thus, the Trp residue slows closure in the background of Lys and speeds it in the background of Arg.

The crystal structure of the open channel shows that the side chain of K5 is isolated from the external and internal solutions in an occluded binding site formed by Phe above and Glu and Asp below. Glu and Asp form ionized hydrogen bonds with the Lys amino group (Fig. 1C) (*11*). Because K5 is in direct contact with the Phe, it is understandable that the functional consequence of mutating Phe to Trp could depend on whether Lys or Arg is present at position 5. High conservation of all three amino acids, Phe, Glu, and Asp, among Kv, Nav, Cav, and Hv channels, as well as VSP enzymes, suggests that the occluded site is an important feature of voltage sensors in general (Fig. 1E). A crystal structure of the Phe to Trp mutant of the paddle chimera channel was determined to 2.9 Å (table S1) and shows that the open conformation of the voltage sensor is preserved and that the occluded site remains intact, with the K5 side chain present and Trp replacing Phe (Fig. 3E).

The observations described above lead us to the following hypothesis: The occluded site affects the conformation of the voltage sensor through the strength of its interaction with Lys relative to Arg at position 5. Mutation of either the binding site (Phe to Trp) or the Lys (Lys to Arg) influences gating. The more negative V_m and slower rate of closure observed with the mutation R1R5(W) to R1K5(W) would suggest that Lys binds more tightly relative to Arg in the presence of Trp in the occluded site, which causes the voltage sensor to be stabilized in its open conformation (Fig. 3, B to D).

Lys substitutions stabilize specific conformations of the voltage sensor. If Lys is favored relative to Arg in the occluded site when Phe is mutated to Trp and if the voltage sensor transfers its positively charged residues through this site when it undergoes a conformational change, then it should be possible to stabilize the voltage sensor in specific conformations by substituting Lys at different positions while Trp is present in the binding site. In the presence of Phe with Lys at position 1 [K1R5(F)], the channels open and close rapidly, but in the presence of Trp with Lys at position 1 [K1R5(W)], the channels open slowly and close rapidly (Fig. 4, A and B). That

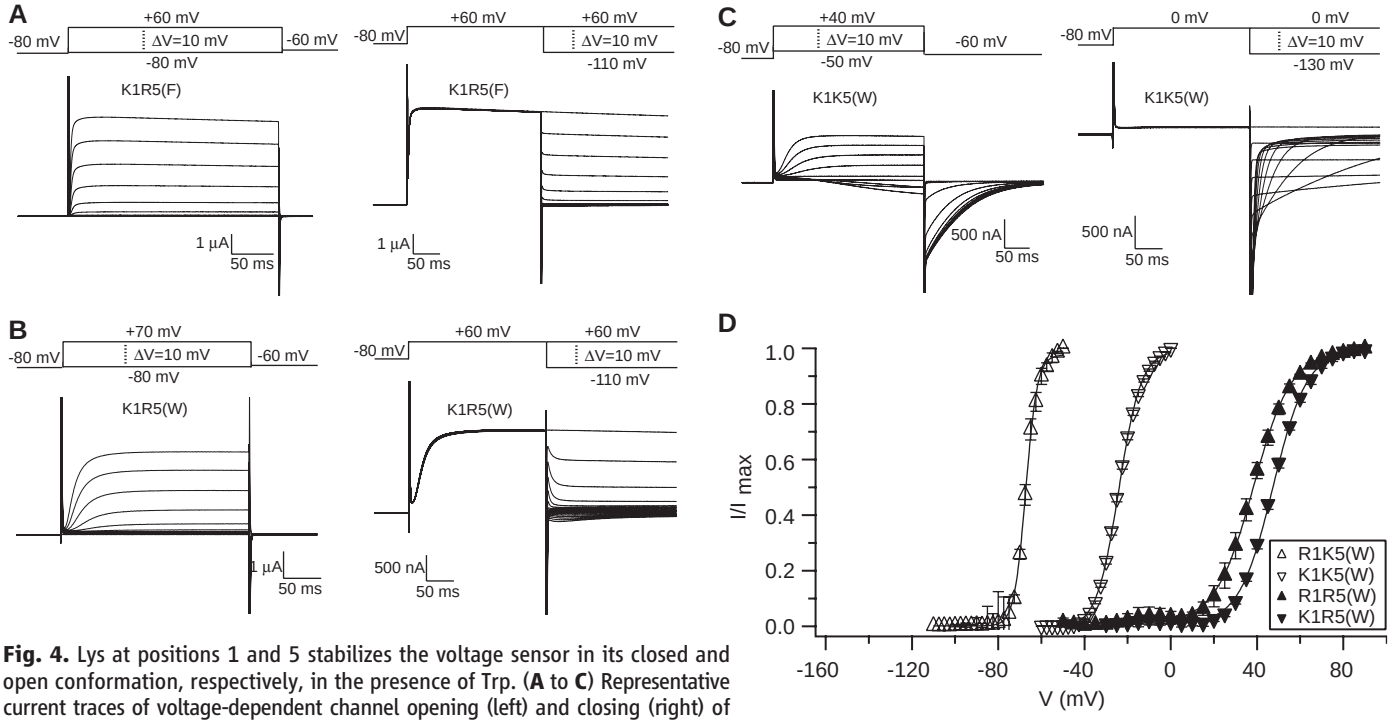

Fig. 4. Lys at positions 1 and 5 stabilizes the voltage sensor in its closed and open conformation, respectively, in the presence of Trp. (**A** to **C**) Representative current traces of voltage-dependent channel opening (left) and closing (right) of K1R5(F), K1R5(W), and K1K5(W). The corresponding pulse protocols are shown above the traces. (**D**) The voltage activation curves of R1K5(W), K1K5(W), R1R5(W), and K1R5(W). Fraction of the maximal current (I/I_{max}, means ± SEM) is plotted as a function of the depolarization voltage and fitted with the two-state Boltzmann function [see (*26*), R1K5(W), n = 9; K1K5(W), n = 11; R1R5(W), n = 5; and K1R5(W), n = 7].

is, the Phe to Trp mutation slows opening (but not closing) when Lys is present at position 1, and it slows closing (but not opening) when Lys is present at position 5. When Lys is present at positions 1 and 5 simultaneously, both channel opening and closing are slowed (Fig. 4C and fig. S2B). The activation curve midpoint voltage, V_m, is most negative for R1K5(W), most positive for K1R5(W), and intermediate for K1K5(W) (Fig. 4D). These results are consistent with the hypothesis that Lys at position 5 favors the open conformation and Lys at position 1 favors the closed conformation.

Voltage sensor conformations assessed through gating currents. Ionic currents associated with pore opening and closing, as described above, provide an indirect measure of voltage sensor conformational change. Gating currents, however, provide a direct measure, because they result directly from the displacement of the charged amino acids in the voltage sensor when it changes its conformation (*4*). Gating currents are measurable as a component of the transient current that follows a membrane voltage step (fig. S3) (*6*). Agitoxin2 was used to prevent ionic (K^+) currents, because this toxin blocks the pore but does not interfere with voltage sensor movements (fig. S3B) (*6*, *32*). Integration of the remaining transient current gives the total charge associated with each voltage step, which can be graphed as a function of membrane voltage in a *Q-V* plot (fig. S3, C and D). *Xenopus* oocytes not expressing Kv channels show a linear *Q-V* plot (fig. S3C), which reflects the charge required to bring the membrane to its new voltage (the linear capacitive charge). Oocytes expressing Kv channels show the same linear component as well as a nonlinear component. The nonlinear component—the gating charge—corresponds to the displacement of charged amino acids as the voltage sensor undergoes its conformational change (fig. S3D).

Transient currents during a single voltage step are shown in Fig. 5, A to D, for the four mutants analyzed in Fig. 4D. In the R1R5(W) channel, the transient currents associated with opening (voltage stepped from hyperpolarized to depolarized value) and closing (voltage stepped back to hyperpolarized value) are brief, and consequently, the gating current is buried within the linear capacitive current (Fig. 5A). In contrast, the transient current associated with closing the R1K5(W) channel has a prolonged component that extends beyond the duration of the linear capacitive current (Fig. 5B). This is direct evidence that the voltage sensor is being delayed in its transition from its open to closed conformation. The K1R5(W) channel has a prolonged component associated with channel opening (Fig. 5C), and the K1K5(W) channel has a prolonged component associated with both opening and closing (Fig. 5D). Therefore, the voltage sensor is delayed in its closed-to-open transition when Lys is present at position 1 and delayed in its open-to-closed transition when Lys is present at position 5. The time course of the transient current during opening and closing in Fig. 5D is consistent with a conformational change of the voltage sensor that involves multiple sequential steps after an initial delay (Fig. 6, A and B).

The *Q-V* plots with the linear capacitive component subtracted are shown in Fig. 5E for the same mutant channels. The quantity Q/Q_{max} is the fraction of total gating charge following a voltage step. When Q/Q_{max} is small, corresponding to small displacements of the voltage sensor from its closed conformation, the four plots fall into two groups: one that shows charge movement at very negative voltages (around –100 mV) and another that begins to move charge at less negative voltages (around –50 mV) (Fig. 5E). The two groups correspond to voltage sensors with Arg (more negative, filled symbols) or Lys (less negative, empty symbols) at position 1. When Q/Q_{max} is large, corresponding to small displacements of the voltage sensor from its open conformation, again two groups are observed, but this time depending on the residue at position 5: Voltage sensors with Arg at position 5 (Fig. 5E, circles) exhibit a distinct second component of charge movement compared with voltage sensors with Lys at position 5 (Fig. 5E, squares).

The *Q-V* plots are consistent with the hypothesis that Lys relative to Arg interacts more favorably with the occluded site (Fig. 5E). Near the voltage sensor's closed conformation the occluded site presumably binds to positively charged S4 amino acids near position 1. If Lys is present at position 1 and binds more favorably than Arg, then a more depolarized membrane voltage (i.e., less negative) should be required to drive the voltage sensor away from its closed and to its open conformation. Near the voltage sensor's open conformation, the occluded site presumably binds to positively charged S4 amino acids near position 5. Therefore, Lys at position 5 should stabilize the open conformation, whereas Arg should destabilize it. As a consequence, in the presence of Arg at position 5, a more positive membrane voltage should be required to force the voltage sensor through its final transition to its

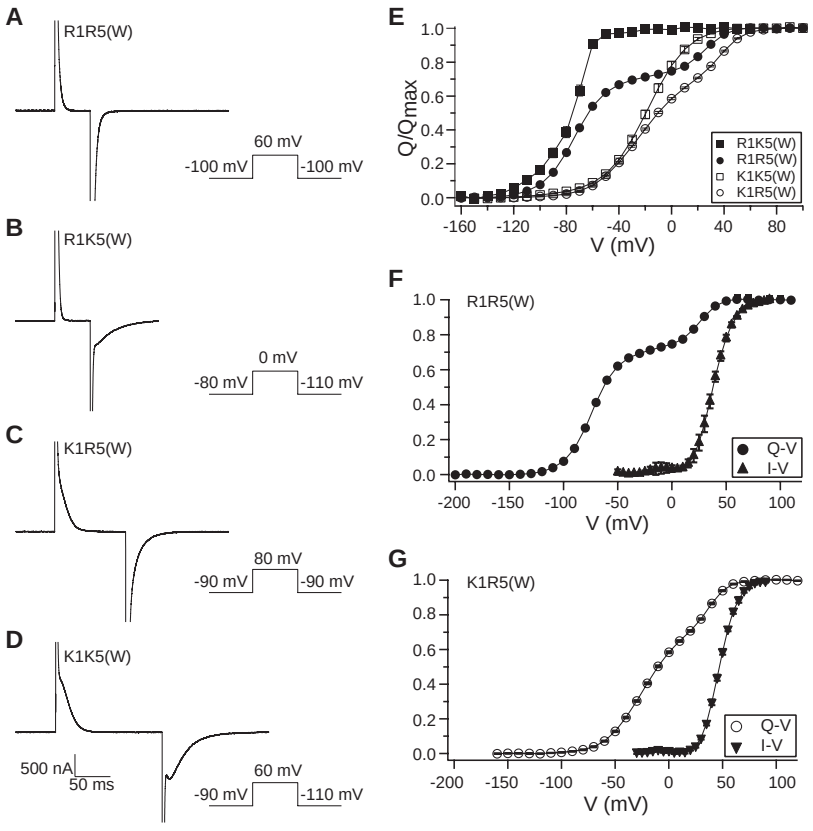

Fig. 5. Voltage-sensor movements assessed by gating currents. (**A** to **D**) Representative transient current traces after voltage steps are shown for R1R5(W), R1K5(W), K1R5(W), and K1K5(W). Corresponding pulse protocols are shown next to the traces. Ionic currents are blocked using at least 50 μM Agitoxin2, and baselines were corrected by subtracting the Agitoxin2-insensitive current (*26*). (**E**) *Q-V* plots of the four mutants in (A to D). Total gating charges, calculated by integrating the repolarization-induced transient currents over time and subtracting the linear capacitive component, were plotted as a function of the step voltage [see (*26*), R1R5(W), n = 11; R1K5(W), n = 13; K1R5(W), n = 24; and K1K5(W), n = 22]. (**F**) *Q-V* (Q/Q_{max}) and *I-V* (I/I_{max}) plots of the R1R5(W) channel. Note that I/I_{max} in the *I-V* plot does not represent the true open probability of the channel, and the same applies to (G). (**G**) *Q-V* and *I-V* plots of the K1R5(W) channel.

open conformation. This final transition appears to correlate with a distinct second component of charge movement. The second component, visible in both the R1R5(W) and K1R5(W) channels, accounts for ~25% of the total gating charge movement. In both channels, the pore opens, and ions begin to conduct only in association with this second component (Fig. 5, F and G).

Discussion. In summary, the data support the following conclusions: (i) Phe^{233} forms the extracellular lid on an occluded binding site in voltage sensors into which S4 positive charges bind. (ii) Mutating Phe to Trp alters the relative strength of interaction between Arg or Lys and this site. (iii) Lys appears to interact more favorably compared to Arg in the presence of Trp: At position 5, Lys stabilizes the open voltage sensor conformation; at position 1, Lys stabilizes the closed voltage sensor conformation. (iv) Given that Lys at position 1 and at position 5 appears to interact with the site in the closed and open conformations, respectively, we propose that the occluded site serves as a catalytic center to lower the energy associated with the transfer of each of the voltage sensor charges as they cross the membrane. (v) Arg at position 5 isolates the last 25% of gating charge as a separate component in the *Q-V* plot, which occurs concomitantly with pore opening. The association of this last component of gating charge with pore opening suggests that binding of the charged residue at position 5 into the occluded site is required for pore opening.

A simple-state model of voltage sensor transitions is shown (Fig. 6A). Each of the five states, connected by four transitions, corresponds to conformations of a single voltage sensor associated with the positively charged residue at positions 1 through 5 inside the occluded site. Thus, state 1 represents the fully closed voltage sensor, in which the positive charge of the position 1 amino acid binds to the occluded site, and state 5 represents the open voltage sensor, in which the positive charge of the position 5 amino acid binds to the occluded site. The data do not uniquely define each transition in this model, so the following simplifying assumptions are made. A single value for the forward rate constants and a single value for the backward rate constants are used except for the rate constants describing the fourth transition connecting states 4 and 5. Voltage dependence is distributed over the four transitions equally, with 25% of the total gating charge in each. It is further assumed that the open pore corresponds to the condition in which all four voltage sensors are open (i.e., all four have reached state 5) and that four voltage sensors undergo independent conformational changes.

For illustrative purposes, the graphs below the state model depict chemical free energy as a function of voltage sensor reaction coordinate in a channel in which Phe has been mutated to Trp (Fig. 6A). The presence of Lys in the occluded site is represented as a deeper energy well relative to Arg. One physical interpretation is that Lys binds more tightly to the occluded site. Another interpretation is that the energy barriers and wells are higher for Arg relative to Lys. Equations for the scheme in Fig. 6A (*26*) generate the main features observed in the electrophysiology data (Fig. 6, B to D). Notably, by changing only the well depth of state 5 by ~4.6 RT (R is the gas constant, T is the absolute temperature) relative to all other barriers and wells, the qualitative features of both the gating current time course and the *Q-V* plots of R1K5(W) and R1R5(W) are recapitulated (Fig. 6, B to D). In particular, relative stabilization of state 5 with Lys in the presence of Trp [R1K5(W)] prolongs the gating current associated with channel closing and gives it the correct time-dependent shape (Fig. 6, B and C), whereas destabilization of state 5 with Arg in the presence of Trp [R1R5(W)] speeds the gating current and separates the *Q-V* plot into two components (Fig. 6, B and D).

The model captures an important feature of gating, most explicitly displayed in channels with Arg at position 5 [R1R5(W) and K1R5(W)]: multiple transitions occur within each voltage sensor (connecting states 1 through 4 in the model) before a final transition (state 4 to 5), which is closely associated with pore opening (Fig. 5, F and G, and Fig. 6D). Thus, according to the model, the closed channel is actually associated with a distribution of conformations (states 1 through 4 within each voltage sensor), which is a function of the degree to which the membrane is hyperpolarized: The more negative the voltage, the closer the distribution comes to state 1. The open channel, however, is associated with a specific conformation (state 5) that must be achieved by all four voltage sensors. In order to approximate the behavior of the electrophysiology data, we found it necessary to use unique forward and backward rate constants for the fourth (final) voltage sensor transition (*26*). We speculate that this final transition is very different because it is associated with opening the pore.

In the context of the crystal structure, the model can explain a discrepancy between the total gating charge per channel (~14 elementary charges) and the sum of reduced charges when each of the five positions is mutated to a neutral amino acid one at a time (~18 elementary charges) (*6*). Because of the presence of two carboxylate ligands, the occluded binding site probably requires a positive charge in it at all times—except during brief transitions between states driven by voltage. Therefore, mutations that remove a positive charge from a particular position should reduce measured gating charge for two reasons: because the number of charges transported by the voltage sensor is reduced, and because the distribution of states before and/or after the voltage step is altered (i.e., the starting

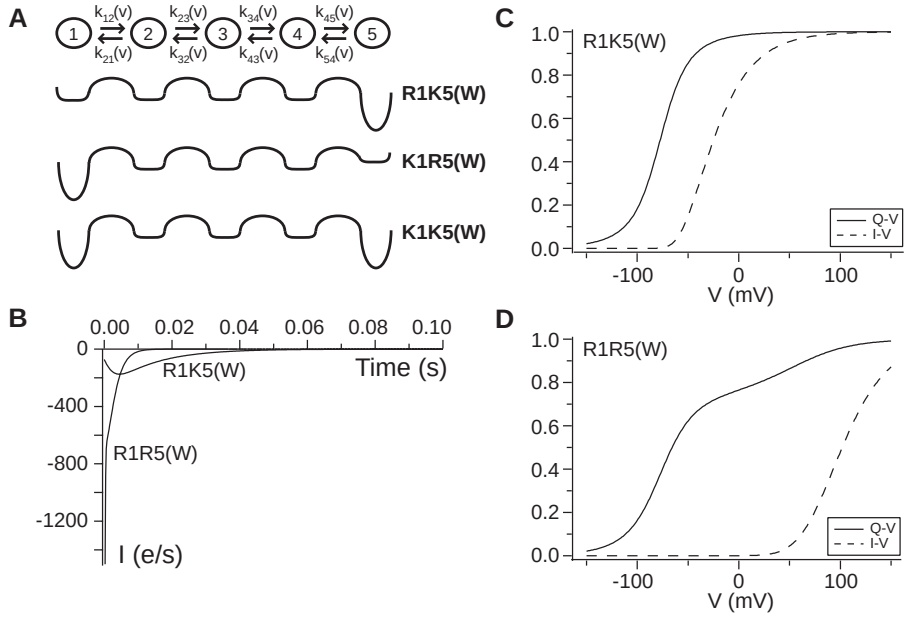

Fig. 6. State model of voltage-sensor conformational change captures qualitative gating behavior. (**A**) A simple model consists of five voltage-sensor states (state 1 though 5) within each voltage sensor connected by four transitions before the final pore opening step. For each state, a different positively charged S4 residue (indicated by the number) is located in the occluded binding site (indicated by the surrounding circle). When all four voltage sensors are in state 5, the pore opens, and ions conduct. The model assumes equal distribution of voltage dependence over the four transitions, and a single forward and a single backward rate constant for the first three transitions. Below the model is a depiction of the energy as a function of the voltage-sensor reaction coordinate in R1K5(W), K1R5(W), and K1K5(W) channels, which illustrates the qualitative effect of Lys on energy well depth when bound in the occluded binding site with Trp. (**B**) The gating current time courses generated from the above model are shown for R1K5(W) and R1R5(W) channels in association with a 100 mV to −120 mV voltage step. (**C** and **D**) The *Q-V* and *I-V* plots of R1K5(W) and R1R5(W) channels generated from the model.

and/or ending positions of all the charges is altered). The two reasons combined can account for the apparent discrepancy between total gating charge and the sum of reduced gating charge by mutation.

We do not know the physical basis of Lys versus Arg discrimination by the occluded site in the Phe to Trp mutant. The case in which Lys binds more favorably to the occluded site is indistinguishable from that in which Arg binds less favorably, because the Boltzmann distribution of states depends only on the relative energy differences among the available states. We favor the idea that Trp causes Arg to bind in the site with lower affinity and also, perhaps, raises the barrier for an Arg to enter the site because Trp is larger than Phe and would be expected to constrict the site, which destabilizes the larger Arg guanidinium group relative to the smaller Lys amino group. A correlation between the size of substituted groups on the Phe side chain (Br > CN > Me > H) and the value of V_m is consistent with this idea (fig. S1).

The data imply a specific distance over which S4 charged amino acids move across the membrane with gating. In the crystal structures of the open conformation, Lys at position 5 is located in the occluded binding site (Figs. 1C and 3E) (*11*). The electrophysiological data suggest that Lys at position 1 binds in the occluded site in the fully closed (strongly hyperpolarized) conformation (Fig. 4). The α-carbon distance between positions 1 and 5 is 21 Å along the S4 helix and 18 Å perpendicular to the membrane (fig. S4). This distance falls within the range 15 to 20 Å inferred independently by biotin-avidin accessibility studies on a prokaryotic Kv channel (*18*, *19*).

This study identifies an occluded site, conserved in voltage sensors, that catalyzes the transfer of positive charges across the membrane field in the process of voltage sensing. By manipulating the structure of the site, we have altered its selectivity between Arg and Lys. This selectivity is used to stabilize the voltage sensor in specific conformations and to dissect the relation between the voltage sensor and pore conformational changes.

References and Notes

1. B. Hille, *Ion Channels of Excitable Membranes* (Sinauer, Sunderland, MA, 2001).
2. Y. Okamura, Y. Murata, H. Iwasaki, M. Sasaki, *Tanpakushitsu Kakusan Koso* **51**, 18 (2006).
3. Y. Murata, H. Iwasaki, M. Sasaki, K. Inaba, Y. Okamura, *Nature* **435**, 1239 (2005).
4. C. M. Armstrong, F. Bezanilla, *J. Gen. Physiol.* **63**, 533 (1974).
5. S. A. Seoh, D. Sigg, D. M. Papazian, F. Bezanilla, *Neuron* **16**, 1159 (1996).
6. S. K. Aggarwal, R. MacKinnon, *Neuron* **16**, 1169 (1996).
7. N. E. Schoppa, K. McCormack, M. A. Tanouye, F. J. Sigworth, *Science* **255**, 1712 (1992).
8. Y. Jiang *et al.*, *Nature* **423**, 33 (2003).
9. S. B. Long, E. B. Campbell, R. MacKinnon, *Science* **309**, 897 (2005).
10. S. B. Long, E. B. Campbell, R. MacKinnon, *Science* **309**, 903 (2005).
11. S. B. Long, X. Tao, E. B. Campbell, R. MacKinnon, *Nature* **450**, 376 (2007).
12. C. A. Ahern, R. Horn, *Neuron* **48**, 25 (2005).
13. A. Cha, G. E. Snyder, P. R. Selvin, F. Bezanilla, *Nature* **402**, 809 (1999).
14. B. Chanda, O. K. Asamoah, R. Blunck, B. Roux, F. Bezanilla, *Nature* **436**, 852 (2005).
15. K. S. Glauner, L. M. Mannuzzu, C. S. Gandhi, E. Y. Isacoff, *Nature* **402**, 813 (1999).
16. D. J. Posson, P. Ge, C. Miller, F. Bezanilla, P. R. Selvin, *Nature* **436**, 848 (2005).
17. D. M. Starace, F. Bezanilla, *Nature* **427**, 548 (2004).
18. V. Ruta, J. Chen, R. MacKinnon, *Cell* **123**, 463 (2005).
19. Y. Jiang, V. Ruta, J. Chen, A. Lee, R. MacKinnon, *Nature* **423**, 42 (2003).
20. H. P. Larsson, O. S. Baker, D. S. Dhillon, E. Y. Isacoff, *Neuron* **16**, 387 (1996).
21. S. Y. Lee, A. Banerjee, R. MacKinnon, *PLoS Biol.* **7**, e47 (2009).
22. A. Banerjee, R. MacKinnon, *J. Mol. Biol.* **381**, 569 (2008).
23. Single-letter abbreviations for the amino acid residues are as follows: A, Ala; C, Cys; D, Asp; E, Glu; F, Phe; G, Gly; H, His; I, Ile; K, Lys; L, Leu; M, Met; N, Asn; P, Pro; Q, Gln; R, Arg; S, Ser; T, Thr; V, Val; W, Trp; and Y, Tyr.
24. I. S. Ramsey, M. M. Moran, J. A. Chong, D. E. Clapham, *Nature* **440**, 1213 (2006).
25. M. Sasaki, M. Takagi, Y. Okamura, *Science* **312**, 589 (2006).
26. Materials and methods are available as supporting material on *Science* Online.
27. N. E. Schoppa, F. J. Sigworth, *J. Gen. Physiol.* **111**, 313 (1998).
28. L. D. Islas, F. J. Sigworth, *J. Gen. Physiol.* **114**, 723 (1999).
29. W. N. Zagotta, T. Hoshi, R. W. Aldrich, *J. Gen. Physiol.* **103**, 321 (1994).
30. W. N. Zagotta, T. Hoshi, J. Dittman, R. W. Aldrich, *J. Gen. Physiol.* **103**, 279 (1994).
31. T. Hoshi, W. N. Zagotta, R. W. Aldrich, *J. Gen. Physiol.* **103**, 249 (1994).
32. M. L. Garcia, M. Garcia-Calvo, P. Hidalgo, A. Lee, R. MacKinnon, *Biochemistry* **33**, 6834 (1994).

33. We thank members of D. Gadsby's laboratory (Rockefeller University) for assistance with oocyte preparation; members of the MacKinnon laboratory for assistance; the staff at beamline X29 (National Synchrotron Light Source, Brookhaven National Laboratory) for advice at the synchrotron; and A. Banerjee, J. A. Letts, G. von Heijne (Stockholm University), and J. Chen (Purdue University) for helpful discussions. R.M. is the Investigator in the Howard Hughes Medical Institute. D.A.D. is a George Grant Hoag Professor of Chemistry. Supported by NIH GM43949 to R.M and NS 34407 to D.A.D. The x-ray crystallographic coordinates and structure factor files have been deposited in the Protein Data Bank with accession ID 3LNM.

Supporting Online Material

www.sciencemag.org/cgi/content/full/328/5974/67/DC1
Materials and Methods
Figs. S1 to S4
Table S1
References

14 December 2009; accepted 16 February 2010
10.1126/science.1185954

REPORTS

Evidence for Strong Extragalactic Magnetic Fields from Fermi Observations of TeV Blazars

Andrii Neronov* and Ievgen Vovk

Magnetic fields in galaxies are produced via the amplification of seed magnetic fields of unknown nature. The seed fields, which might exist in their initial form in the intergalactic medium, were never detected. We report a lower bound $B \geq 3 \times 10^{-16}$ gauss on the strength of intergalactic magnetic fields, which stems from the nonobservation of GeV gamma-ray emission from electromagnetic cascade initiated by tera–electron volt gamma rays in intergalactic medium. The bound improves as $\lambda_B^{-1/2}$ if magnetic field correlation length, λ_B, is much smaller than a megaparsec. This lower bound constrains models for the origin of cosmic magnetic fields.

The problem of the origin of 1- to 10-μG magnetic fields in galaxies and galaxy clusters is one of the long-standing problems of astrophysics and cosmology [see (*1*–*4*) for reviews]. It is assumed that the observed magnetic fields result from the amplification of much weaker seed fields. However, the nature of the initial weak seed fields is largely unknown. There are two broad classes of models for the seed fields: astrophysical models, which assume that the seed fields are generated by motions of the plasma in (proto)galaxies, and cosmological models, in which the seed fields are produced in the early universe (*1*–*4*).

Extremely weak unamplified extragalactic magnetic fields (EGMFs) have escaped detection up to now. Measurements of the Faraday rotation in the polarized radio emission from distant quasars (*1*, *5*, *6*) and/or distortions of the spectrum and polarization properties in the cosmic microwave background (CMB) radiation (*7*–*18*) imply upper limits on EGMF strengths at the level of ~10^{-9} G. Numerical modeling of magnetic field formation in galaxy clusters implies a theoretical upper bound of the order of

ISDC Data Centre for Astrophysics, Geneva Observatory, Ch. d'Ecogia 16, Versoix 1290, Switzerland.

*To whom correspondence should be addressed. E-mail: Andrii.Neronov@unige.ch